# Structure and quenching of a bundle-shaped phycobilisome

Anna D. Burtseva[1,2a], Yury B. Slonimskiy[1a], Timur N. Baymukhametov[3], Maria A. Sinetova[4], Daniil A. Gvozdev[5], Georgy V. Tsoraev[5], Dmitry A. Cherepanov[6,7], Eugene G. Maksimov[5], Vladimir O. Popov[1], Konstantin M. Boyko[1], Nikolai N. Sluchanko[1,*]

[1] A.N. Bach Institute of Biochemistry, Federal Research Center of Biotechnology of the Russian Academy of Sciences, Moscow 119071, Russia
[2] Moscow Center for Advanced Studies, Kulakova Str. 20, Moscow 123592, Russia
[3] Kurchatov Complex of NBICS Nature-Like Technologies, Structural Biology Department, National Research Center "Kurchatov Institute", Akademika Kurchatova pl., 1, Moscow 123182, Russia
[4] K.A. Timiryazev Institute of Plant Physiology Russian Academy of Sciences, 127276 Moscow, Russia
[5] M.V. Lomonosov Moscow State University, Faculty of Biology, 119991 Moscow, Russia
[6] N.N. Semenov Federal Research Center for Chemical Physics, Russian Academy of Sciences, Moscow, Russia
[7] A.N. Belozersky Institute of Physical-Chemical Biology, Moscow State University, Moscow, Russia

a – co-first
*Corresponding author:
Nikolai N. Sluchanko
A.N. Bach Institute of biochemistry
Federal Research Center of Biotechnology of the Russian Academy of Sciences
Leninsky prospect 33, building 1
119071 Moscow, Russian Federation
Tel.: +74956603430
Email: nikolai.sluchanko@mail.ru

**Abstract**

Cyanobacteria use soluble antenna megacomplexes, phycobilisomes (PBS), to maximize light-harvesting efficiency and small photoswitchable orange carotenoid proteins (OCPs) to down-regulate PBS in high light. Among known PBS morphologies, the one from the basal cyanobacterial genus *Gloeobacter* still lacks detailed structural characterization. Here, we present the cryo-EM structure of the *G. violaceus* PBS, a >10-MDa complex with a unique architecture consisting in 516 polypeptide chains totaling nearly 90,000 residues and harboring over 860 bilin chromophores. This unique PBS features diverging, conformationally mobile bundles of rods composed of stacked phycoerythrin and phycocyanin hexamers, stemming from a pentacylindrical allophycocyanin core belted by auxiliary phycocyanin hexamers. We show how two *Gloeobacter*-specific multidomain linker proteins, Glr1262 and Glr2806, maintain this bundle-shaped architecture and reveal its differential regulation via non-photochemical quenching by two OCP types of *G. violaceus* that recognize separate binding sites within the allophycocyanin core, including lateral cylinders absent in tricylindrical cores. Our findings provide the high-resolution structural insight into *Gloeobacter* PBS and its regulation, revealing divergent adaptations in early-branching cyanobacteria. The structure advances understanding of PBS diversity and

evolution, offering a framework for bioengineering light-harvesting systems in synthetic biology and biotechnological applications.

**Keywords**
Phycobiliproteins, light-harvesting complexes, evolution

Light absorption is the first step in photosynthesis, and photosynthetic organisms have evolved various mechanisms to improve its efficiency. Cyanobacteria and red algae use extramembranous antenna megacomplexes called phycobilisomes (PBS), composed of phycobiliproteins (PBPs), to harvest light. PBPs covalently bind bilins, which are open-chain tetrapyrroles (*1*). Bilins absorb light in different spectral regions and transfer energy to the reaction centers of photosystems (*2–4*). This compensates for chlorophyll's limited ability to absorb light at short wavelengths (*5*). The efficient funneling of energy absorbed by bilins in PBPs is enabled by structural organization of PBS. PBPs are composed of heterodimeric αβ protomers, often designated "monomers", which oligomerize into ring-like trimers $(\alpha\beta)_3$ and hexamers $(\alpha\beta)_6$. These further assemble with the help of linker proteins that interact with the PBP-rings in their cavities. A typical PBS contains an allophycocyanin (AP) core – two (*6*), three (*7*), or five (*8*) cylinders of $(\alpha\beta)_3$ trimers of AP – and a set of radiating rods – stacks of hexamers formed by αβ protomers of phycocyanin (PC) and, in red algae and some cyanobacteria, phycoerythrin (PE) (*1*, *9*, *10*). AP, PC, and PE differ in the number of bilins bound to their α (one in AP and PC, or two in PE) and β (one in AP, two in PC, and three in PE) subunits. The three main bilin types in cyanobacterial PBS are phycocyanobilin (PCB, found in AP and PC), phycoerythrobilin (PEB), and phycourobilin (PUB) (both found in PE) (*1*), whose collective absorbance covers the visible spectral range that is poorly accessible to chlorophyll.

Known PBS in red algae are hemi-ellipsoidal/block-type (*10*, *11*), whereas in cyanobacteria the prevalent PBS form is hemi-discoidal (*1*). In addition, the paddle-shaped PBS was recently described in the relict cyanobacterium *Anthocerotibacter panamensis* UTEX 3164, which utilizes single PC hexamers and chains of staggered PC hexamers that surround a heptacylindrical AP core instead of rods (*5*). A unique case is the cyanobacterium *Gloeobacter violaceus* PCC 7421 (hereafter, *G. violaceus*), which diverged from the crown cyanobacteria the earliest (~2 billion years ago). *G. violaceus* is characterized by slow metabolism and growth; primitive bacterial-type carotenoid biosynthesis; an inability to stably maintain intracellular pH; and a lack of circadian clock and thylakoids (*12*, *13*). PBS in *G. violaceus* attach to the photosystems localized in the plasma membrane (*12*, *14*). Although bundle-type PBS were first described in 1981 (*12*), they remain the only known PBS morphology without a high-resolution structure. The regulation of the bundle-shaped PBS in high light also remains unknown.

## 1. Cryo-electron microscopy of the bundle-shaped *G. violaceus* PBS

The *G. violaceus* culture exhibited an absorbance spectrum with peaks at 500, 560, and 620 nm, corresponding to PBPs. Small features were also present at 440 and 680 nm, indicating relatively low chlorophyll content (Fig. 1A) (*14*). *G. violaceus* PBS (hereafter, GviPBS), which was isolated via sucrose gradient ultracentrifugation (Fig. 1B), exhibited the same prominent absorbance bands as PBPs, reflecting the presence of PUB (500 nm), PEB (560 nm), and PCB (an excitonic peak at 650 nm and a shoulder at 620 nm) (Fig. 1A). The first two of these are more prevalent in red algae than in cyanobacteria (*1*, *11*). All resolved cyanobacterial PBS structures contain only PCB and no other bilin types (*1*). PBPs could be biochemically separated into three distinct PBP fractions, corresponding to PE, PC, and AP, according to their absorbance and fluorescence spectra (Fig. 1C). The presence of PBPs and all linker proteins, including *Gloeobacter*-specific multidomain linkers Glr1262 and Glr2806, was confirmed by SDS-PAGE and mass spectrometry (Fig. S1 and Table S1).

To preserve the intact PBS for cryo-EM, we performed ultracentrifugation in parallel gradients of sucrose and glutaraldehyde (GraFix (*15*)) (Fig. S1). To improve the quality of the cryo-EM density map, we focused on a set of substructures for model building and refinement against the masked map. This resulted in six focused maps with resolutions ranging from 2.72 □ to 3.67 □ (Table S2, Fig. S2, S3). The refined substructures were then combined to create a model of the entire PBS and fitted into the composite cryo-EM map (Fig. 1D).

For the GviPBS model, we used the crystallographic structures of $(\alpha\beta)_6$ hexamers of AP (PDB 2vjt), PC (PDB 2vjr) and PE (PDB 2vjh) (Fig. S4) and available electron microscopy and mutagenesis data (*16*). The reconstructed cryo-EM structure revealed three pairs of C2-symmetry-related rods stemming from the top of the pentacylindrical AP core (R1/R1', R2/R2', R3/R3') (Fig. 1D,E). The AP core contains two antiparallel bottom cylinders (A/A'), a top cylinder (B) and two lateral AP $(\alpha\beta)_6$ hexamers (C/C'), which are attached sideways to the top B cylinder. This "3+2" AP core can be superimposed on the pentacylindrical cores in hemi-discoidal PBS from *Anabaena* sp. PCC 7120 (*8*) and *Thermosynechococcus vulcanus* NIES-2134 (*17*) as well as on the lower portion of the heptacylindrical AP core in *A. panamensis* PBS (*5*) (Fig. S5). In GviPBS, the "3+2" core extends to the sides with additional PC $(\alpha\beta)_6$ hexamers (Rx1/Rx1') that lie coaxially with the C/C' $(\alpha\beta)_6$ hexamers of AP and support the rods (Fig. 1D).

The cryo-EM map of the rods dispersed more towards the periphery. Prior work revealed that deleting PE subunits results in a shorter GviPBS morphology, with rods containing three PC $(\alpha\beta)_6$ hexamers in height (*16*). Although two PC $(\alpha\beta)_6$ hexamer stacks could be confidently built in each rod, the density of the third PC hexamer and PE $(\alpha\beta)_6$ hexamers only permitted approximate placement (Fig. 1D). Two $(\alpha\beta)_6$ hexamers of PE (PDB 2vjh) could be docked in the rods R1/R1' and R3/R3', whereas three PE $(\alpha\beta)_6$ hexamers could be docked in the rods R2/R2', for a total of 18 PC and 14 PE $(\alpha\beta)_6$ hexamers in the rods of the composite model. Unexpectedly, the rods formed two bundles (R1-R2-R3 and R1'-R2'-R3') that radiated at ~15° angle so that the first-level PE $(\alpha\beta)_6$ hexamers in rods R2/R2' became ~145 □ apart (Fig. 1D,E). Each rod bundle formed a superhelix with a period of ~1000 □ (Fig. S6). Two maps supporting different bundle conformations allow us to imagine movement of the bundles relative to each other (Fig. S7 and Movie S1).

The cryo-EM map permitted confident modeling of seven AP $(\alpha\beta)_6$ hexamers out of eight, while the fourth $(\alpha\beta)_3$ trimer was absent from both bottom AP cylinders (Fig. 1D), similar to *T. vulcanus* PBS (PDB 7vea) (*17*). The absence of the fourth $(\alpha\beta)_3$ trimer may be due to its loss during sample preparation (*1*, *17*, *18*), though light-controlled reconfiguration of the PBS architecture is also possible (*19*). Notably, the missing trimer would contain ApcD, one of the terminal emitters responsible for the energy transfer to the photosystems in other PBS (*6–8*). Mass spectrometry confirmed that both minor PBPs, ApcD (α-chain) and ApcF (β-chain), were present in our GviPBS preparations (Table S1). Since no justification based on density alone was found for an alternative location of ApcD (instead of the common location in the fourth trimer), ApcD was not included in our models. ApcF was modeled in its expected position in the third AP trimer of the basal cylinders (*6–8*), although the corresponding density did not allow us to distinguish it unambiguously from ApcB because the two proteins are highly identical (70.8%). Notably, *A. panamensis* PBS naturally lacks ApcD and ApcF (*5*). Similarly, deleting either gene does not affect the functionality or regulation of PBS in *Synechocystis* sp. PCC 6803 (hereafter *Synechocystis* 6803) (*20*). Thus, we assume that the fourth ApcD-containing AP trimer is dispensable for GviPBS functioning.

The AP core width is narrower than the lower level of the rods (Fig. 1D). However, blurred density proximal to Rx1/Rx1' suggests the tentative placement of Rx2/Rx2' (Fig. S8). Consistent with the mutagenesis data (*16*), we hypothesize that there are up to three Rx hexamers on each side of the core. The third Rx substructure is likely too dynamic to have a distinct density (Fig. S8). The tentative positioning of three Rx hexamers is sterically compatible with the lateral stacking of GviPBS into arrays, similar to those of PBS in crown cyanobacteria (*3*, *7*) (Fig. S8). This scenario is most probable in thylakoid-less *G. violaceus* because it saves space on the plasmalemma, which accommodates all photosynthetic complexes in this organism (*12*, *14*).

## 2. Linker proteins

The reconstructed GviPBS structure contains 82 $(\alpha\beta)_3$ trimers of PBP and 864 bilins. It is the largest resolved cyanobacterial PBS, with dimensions of 450x550 □, exceeding those of paddle-like and hemi-discoidal PBS (Fig. 1E). The bundle-shaped morphology is maintained by linker proteins (Fig. 2A), including the multidomain linkers Glr1262 and Glr2806, which are unique to *Gloeobacter* (*16*, *21*, *22*). Each is predicted to have three pfam00427 (REP) domains in its sequence (*16*, *21*). Nevertheless, these proteins are only 58.4% identical to each other and are dissimilar to the functional analogs CpcG and CpcL from *Synechocystis* 6803 (<30% sequence identity). We identified the precise location of Glr1262 and Glr2806 REP domains by cryo-EM density for non-conserved amino acids (Fig. S9, S10). Glr2806 is responsible for attaching Rx to the core (*16*). Its long N-terminal arm interacts with the A/A' and C/C' cylinders, while its REP1 domain binds inside the Rx1/Rx1' cavity (Fig. 2A-C). The REP2-REP3 domains of Glr2806 are expected to tether two additional Rx copies, Rx2/Rx2' and Rx3/Rx3', to the core (Fig. S8) (*16*). Although mass spectrometry could not cover the entire Glr2806 sequence (Table S1), our data unequivocally confirm Glr2806's role in attaching Rx structures to the core (Fig. 2B). Interestingly, Glr2806 of *G. morelensis* MG652769 also contains three REP domains, but the *G. kilaueensis* JS1 homolog lacks one (Fig. S11). This suggests that three Rx hexamers are not necessary for bundle-shaped PBS assembly.

The Glr1262 linker is also predicted to have three pfam00427 domains, which enable the interaction with three PBP hexamers. Each REP domain of Glr1262 is superimposable with Glr2806 REP1 (0.6-1 □ Cα RMSD; Fig. S12). The density helped unequivocally localize Glr1262 on the first level of PC hexamers in the rods, consistent with its predicted position (*16*). The three REP domains (pfam00427) of Glr1262 were identified at vertices of an equilateral triangle, which corresponded to the cavities of three PC hexamers that formed the base of a rod bundle (Fig. 2C). Although incomplete density prevented tracing the entire Glr1262 chain, assigning REP domains to a Glr1262 copy that connects neighboring PC hexamers within the rod bundle appears to be the most reasonable option. Two copies of Glr1262, each with three REP domains, are necessary and sufficient to cluster the six rods symmetrically into two triangular rod bundles. Each triangle is centered at the top side of the C/C' cylinder of AP (Fig. 2C). In the absence of a CpcG homolog in the genome, a rod-core linker found in studied cyanobacteria, Glr1262 apparently plays this role in *Gloeobacter* (*16*, *21*). Indeed, the REP1-REP2 arm (residues 280-350) of Glr1262 interacts with the C/C' cylinder residues and the REP2-REP3 arm interacts with the B cylinder of the AP core (Fig. 2D).

We located the conserved rod linkers, CpcC1 and CpcC2 (*22*), which contain pfam01383 and pfam00427 domains that connect two neighboring PC layers (Fig. 2A, E). According to

mass spectrometry, all small capping linkers were present in the sample (Table S1). However, we could unequivocally localize multiple copies of only the core linker ApcC (Fig. 2A). Their pfam01383 domain is similar to those of other PBS types and to the pfam01383 domain in CpcC1/CpcC2 (Fig. 2E).

The pentacylindrical GviPBS core is assembled by two copies of the core-membrane linker ApcE (or $L_{CM}$), which has four conserved REP domains (pfam00427) that bind within the cavities of four AP hexamers (Fig. 2F). Pfam00427 domains of ApcE are conformationally similar to REP domains of Glr2806, Glr1262 and CpcC1/CpcC2 (<1.6 Å Cα RMSD) (Fig. S12). Although ApcE of GviPBS is conformationally similar to other ApcE proteins from PBS with the pentacylindrical cores, it contains unique unstructured protrusions that potentially interfere with the attachment of the fourth ApcD-containing trimer (Fig. 2F). As in other known cyanobacterial PBS structures, ApcE is the only linker in GviPBS with a chromophore. It is canonically located within the N-terminal domain of ApcE, incorporated into the third AP $(\alpha\beta)_3$ trimer of the basal cylinders as the α subunit.

### 3. Chromophore system

GviPBS is notable for containing not only PCB, but also PEB and PUC chromophores, which give *G. violaceus* its characteristic violet color. PCB is located in AP core and PC hexamers in rods, whereas PEB and PUC are solely located within the upper part of the rods (Fig. 1D). The PEB and PUC chromophores could not be sufficiently resolved in cryo-EM maps; therefore, their conformations and local environments were inferred from the crystal structure of PE (PDB 2vjh). PCB conformations within PC hexamers in rods and AP hexamers in the core were resolved in cryo-EM density map, including the terminal emitting bilin in ApcE (Fig. 3A-E). The three bilin types differ in the number of conjugated double bonds, increasing from PUB to PEB to PCB, which is accompanied by enhanced coplanarity of the pyrroles (Fig. 3F,G). While PCB and PEB are covalently attached to the single conserved cysteines of the α and β subunits, PUB is doubly tethered to two cysteines simultaneously (Fig. 3A-E). The deficit of double bonds between the pyrroles and the two-sided covalent linkage forces PUB to adopt a bent conformation, with A and D rings completely outside the B-C plane (Fig. 3A). This is consistent with the absorbance maximum of ~500 nm for PUB, the shortest among *G. violaceus* PBPs (Fig. 1C) (*9*). PEB has two double bonds in the linkages between the pyrrole rings, with A and D rings displaced on the opposite sides of the B-C plane (Fig. 3B,F), featuring a red-shifted absorbance maximum of 560 nm. PCBs with the three double bonds in the linkages between the four pyrrole rings adopt conformations with different degrees of ring coplanarity and the optional presence of hydrophobic side chains in the vicinity of the D ring. The ApcE bilin conformation has the most coplanar A-B-C-D rings. Its A ring flips from a *ZZZasa* to a *ZZZssa* configuration (*23*), while the D ring remains coplanar due to a π-stacking interaction with the Trp162 side chain (Fig. 3E), missing from PCB-binding sites in other AP or PC hexamers (Fig. 3A-D). Correspondingly, the *ZZZssa* bilin of ApcE is a red-shifted fluorophore with the properties of the terminal emitter (*23*).

The stoichiometry of bilin incorporation (1:1 per αβ protomer of AP, 1:2 per αβ protomer of PC, 2:3 per αβ protomer of PE) establishes a descending bilin concentration gradient from the top to the button of GviPBS (Fig. S13), which may be relevant for intra-PBS excitation energy transfer (EET). EET pathways are typically estimated based on minimal interbilin distances (*5*, *6*, *8*). The bundles of rods position multiple PCB chromophores within 35 Å of each other, which is sufficient for interrod EET. This increases the probability of capturing photons in typical *G. violaceus* habitats (*1*, *14*, *16*). However, the absence of lateral radiating

rods in *G. violaceus*, which enable direct EET to the A/A' core cylinders in crown cyanobacteria (*7*, *8*), suggests peculiarities in rod-core EET in *G. violaceus*.
Remarkably, the minimal distances (~33-35 □) between the rod and core bilins in GviPBS were found to be between the PCBs of the lowest PC hexamers and the upper PCBs of the AP hexamers of C/C' cylinders (Fig. 3H). The corresponding distances involving PCBs of the top B core cylinder are 37-41 □. Furthermore, the coaxial position of PC hexamers Rx1/Rx1' with C/C' core cylinders brings several PCBs of those PC hexamers to distances of 27-31 □ from AP bilins (Fig. 3H). This is expected to substantially facilitate EET and indicates the special relevance of C/C' hexamers (a hallmark feature of the pentacylindrical cores) in receiving energy from rods and auxiliary PC hexamers in GviPBS.

## 4. Non-photochemical quenching of the bundle-shaped PBS

*G. violaceus* grows optimally under low insolation but is known to respond to intense blue light by inducing non-photochemical quenching (NPQ) at the PBS level (*24*). High light threatens to damage the photosynthetic apparatus of cyanobacteria by increasing the risk of the reactive oxygen species formation. To protect themselves, cyanobacteria express a unique orange carotenoid protein (OCP). In high light, OCP converts from an inactive orange (O) into an active red (R) form that binds to the PBS core and dissipates the excess absorbed energy as heat (*7*, *25*). OCP is composed of an N-terminal domain (NTD) and a C-terminal domain (CTD) that share a non-covalently bound ketocarotenoid such as echinenone (ECH) (*26–30*). OCP-mediated photoprotection has been thoroughly studied in vivo (*25*, *31*, *32*) and reconstituted in vitro (*33*); however, the OCP-binding site has only been structurally elucidated for the hemi-discoidal PBS of *Synechocystis* 6803 (SynPBS) (*7*, *34*), which has a tricylindrical AP core (Fig. S14). Nevertheless, OCP-mediated quenching of the pentacylindrical PBS cores should differ, because C/C' core cylinders completely obscure the binding site for one of the OCP subunits (Fig. S14).
There are three main OCP clades: OCP1, OCP2 and OCP3. The latter is subdivided into subclades a, b and c, with OCP3a being the closest to a presumed OCP ancestor (Fig. 4A) (*28*, *30*, *35*, *36*). The only characterized *Gloeobacter* OCP is found in *G. kilaueensis* JS1, which encodes only one OCP type: GkilOCP3a (*35*) (Fig. 4B). *G. morelensis* and *G. violaceus* contain two uncharacterized copies of the full-length OCP3a, which have only 66.6% sequence identity. These variants are designated here as OCP3a_α (apparently equivalent to GkilOCP3a) and OCP3a_β (Fig. S15).
We produced GviOCP3a_α and GviOCP3a_β proteins recombinantly and confirmed that, as expected for native OCP proteins in *Gloeobacter* (*35*), they contained exclusively ECH as the carotenoid. Both proteins were monomeric and exhibited similar absorbance spectra and photoactivity (Fig. S16). To compare PBS quenching by these proteins, we employed steady-state and picosecond time-resolved emission spectroscopy (Fig. 4C,D,E and Fig. S17). OCP1 from *Synechocystis* 6803 (SynOCP1) was used as a control. Since SynPBS are hemi-discoidal with the tricylindrical cores while GviPBS has a pentacylindrical core, we also added OCP representatives of all clades from cyanobacteria with pentacylindrical PBS cores (as assumed from the alignment of their core-type defining ApcE linkers) as controls (Fig. S18). These controls included *Anabaena* sp. ATCC 29413 (AnaOCP1), *Crinalium epipsammum* PCC 9333 (CrinOCP2), *Gloeocapsa* sp. PCC 7428 (GcapOCP2) and *G. kilaueensis* (GkilOCP3a). These OCPs are all known to quench SynPBS upon photoactivation (*35*, *37*, *38*). However, under similar conditions, we found that SynOCP1, AnaOCP1, CrinOCP2 and GcapOCP2 did not affect the fluorescence intensity, maximum

position, or fluorescence lifetime of GviPBS (Fig. 4E, Fig. S19). This indicates that they lost the ability to quench the bundle-shaped PBS during evolution.

Upon photoactivation of GviOCP3a_α, robust quenching of GviPBS fluorescence was observed, which substantially reduced fluorescence of the AP core (~1.9 ns), but not the components responsible for EET from PE to PC (~70 ps) and from PC to AP (~165 ps) (Fig. 4C,D and Fig. S17). Consequently, the GviPBS fluorescence maximum shifted from 663 nm (AP) to 646 nm (PC), indicating GviOCP3a_α binding to the AP core (Fig. 4D,G, Fig. S19). GkilOCP3a, which belongs to a different *Gloeobacter* species, induced similar efficient quenching of GviPBS (Fig. 4E, Fig. S19). Interestingly, both GviOCP3a_α and GkilOCP3a strongly quenched SynPBS as well, just like SynOCP1 did (Fig. S16), suggesting that they share a conserved binding site within the tricylindrical SynPBS core, which is located on the top B cylinder (*7*) (Fig. S14). This Site 1 must be partially preserved in GviPBS to explain its efficient quenching by GviOCP3a_α and GkilOCP3a.

In contrast, GviPBS quenching by GviOCP3a_β was slower and less efficient than by GviOCP3a_α (Fig. 4E,F). This resulted in a partially blue-shifted GviPBS fluorescence maximum (Fig. S19) and unusually altered fluorescence lifetimes (Fig. S16,S17). The fluorescence lifetime of the quenched PBS state may reflect the geometry of the PBS-OCP complex and the mutual orientation of the bilin and the carotenoid (*35*, *37*, *39*), which likely contributes to the observed differences in GviPBS quenching by GviOCP3a_α and GviOCP3a_β. Notably, neither protein affected fluorescence of individual PC and AP samples upon photoactivation (Fig. S19), which underscores the importance of PBS integrity in OCP binding. Nevertheless, our data indicate that GviOCP3a_β accesses different populations of AP chromophores in the core than GviOCP3a_α does, suggesting the existence of a binding site distinct from Site 1. While searching for it, we realized that the OCP footprint at Site 1 on the top B cylinder is also preserved in C/C' cylinder at the junction of two α and one β AP chains (Fig. S14). This tentative Site 2 is spatially separated from Site 1, allowing noncompetitive OCP binding.

To distinguish this from competition between GviOCP3a_α and GviOCP3a_β for overlapping sites, we exploited the markedly different quenching efficiencies of these two proteins. We titrated GviPBS with each protein, empirically determining the OCP/PBS ratio that led to saturated binding. Then, we compared GviPBS quenching at twice the concentration of either OCP, as well as at an equivalent combined concentration of both. This experiment clearly revealed an additive effect of GviOCP3a_α and GviOCP3a_β, which supports our hypothesis and suggests that the altered efficiency of GviOCP3a_β is due to its binding at Site 2 (Fig. 4F,G and Fig. S14). The location of Site 2 on C/C' cylinders, which are unique to PBS cores containing "3+2" cylinders, emphasizes the importance of C/C' cylinders as independent EET pathways and as targets for the regulation by GviOCP3a_β. Interestingly, while GviOCP3a_α and GkilOCP3a induced strong quenching of SynPBS lacking C/C' core cylinders, GviOCP3a_β was completely dysfunctional on SynPBS (Fig. S16). This finding corroborates the existence of multiple binding sites in GviPBS and potentially in other PBS with pentacylindrical cores. We hypothesize that GviOCP3a_α is the most ancestral extant OCP, because it is highly effective on both GviPBS and SynPBS, acting at Site 1. We also hypothesize that GviOCP3a_β is a relatively new type of OCP whose duplication and subsequent evolution enabled the regulation of EET pathways over C/C' cylinders by binding at Site 2.

In summary, we conclude that the additional C/C' cylinders are a unique structural feature of the pentacylindrical core that adds extra EET pathways to A/A' cylinders. In turn, this requires additional solutions to regulate these energy flows. In this regard, having two sites

for different OCPs seems to be a reasonable evolutionary solution, which may also be important for preventing energy migration between neighboring cores, while allowing for targeted energy transfer from rods to A/A' cylinders to fuel the photosynthesis.

**References**


1. D. A. Bryant, C. J. Gisriel, The structural basis for light harvesting in organisms producing phycobiliproteins. *The Plant Cell*, koae126 (2024).

2. L. Chang, X. Liu, Y. Li, C.-C. Liu, F. Yang, J. Zhao, S.-F. Sui, Structural organization of an intact phycobilisome and its association with photosystem II. *Cell Res* **25**, 726–737 (2015).

3. X. Zhang, Y. Xiao, X. You, S. Sun, S.-F. Sui, In situ structural determination of cyanobacterial phycobilisome-PSII supercomplex by STAgSPA strategy. *Nat Commun* **15**, 7201 (2024).

4. X. You, X. Zhang, J. Cheng, Y. Xiao, J. Ma, S. Sun, X. Zhang, H.-W. Wang, S.-F. Sui, In situ structure of the red algal phycobilisome–PSII–PSI–LHC megacomplex. *Nature* **616**, 199–206 (2023).

5. H.-W. Jiang, H.-Y. Wu, C.-H. Wang, C.-H. Yang, J.-T. Ko, H.-C. Ho, M.-D. Tsai, D. A. Bryant, F.-W. Li, M.-C. Ho, M.-Y. Ho, A structure of the relict phycobilisome from a thylakoid-free cyanobacterium. *Nat Commun* **14**, 8009 (2023).

6. Z. Zheng, C. Ma, H. Wang, G. Wang, C. Dong, N. Gao, J. Zhao, The structure of phycobilisome with a bicylindrical core from the cyanobacterium Synechococcus elongatus PCC 7942. bioRxiv [Preprint] (2025). https://doi.org/10.1101/2025.04.28.650843.

7. M. A. Domínguez-Martín, P. V. Sauer, H. Kirst, M. Sutter, D. Bína, B. J. Greber, E. Nogales, T. Polívka, C. A. Kerfeld, Structures of a phycobilisome in light-harvesting and photoprotected states. *Nature* **609**, 835–845 (2022).

8. L. Zheng, Z. Zheng, X. Li, G. Wang, K. Zhang, P. Wei, J. Zhao, N. Gao, Structural insight into the mechanism of energy transfer in cyanobacterial phycobilisomes. *Nat Commun* **12**, 5497 (2021).

9. D. A. Bryant, G. Cohen-Bazire, A. N. Glazer, Characterization of the biliproteins of Gloeobacter violaceus chromophore content of a cyanobacterial phycoerythrin carrying phycourobilin chromophore. *Arch. Microbiol.* **129**, 190–198 (1981).

10. J. Ma, X. You, S. Sun, X. Wang, S. Qin, S.-F. Sui, Structural basis of energy transfer in Porphyridium purpureum phycobilisome. *Nature* **579**, 146–151 (2020).

11. J. Zhang, J. Ma, D. Liu, S. Qin, S. Sun, J. Zhao, S. F. Sui, Structure of phycobilisome from the red alga Griffithsia pacifica. *Nature* **551**, 57–63 (2017).

12. G. Guglielmi, G. Cohen-Bazire, D. A. Bryant, The structure of Gloeobacter violaceus and its phycobilisomes. *Arch. Microbiol.* **129**, 181–189 (1981).

13. T. Tsuchiya, S. Takaichi, N. Misawa, T. Maoka, H. Miyashita, M. Mimuro, The cyanobacterium Gloeobacter violaceus PCC 7421 uses bacterial-type phytoene desaturase in carotenoid biosynthesis. *FEBS Letters* **579**, 2125–2129 (2005).

14. R. Rippka, J. Waterbury, G. Cohen-Bazire, A cyanobacterium which lacks thylakoids. *Arch. Microbiol.* **100**, 419–436 (1974).

15. B. Kastner, N. Fischer, M. M. Golas, B. Sander, P. Dube, D. Boehringer, K. Hartmuth, J. Deckert, F. Hauer, E. Wolf, H. Uchtenhagen, H. Urlaub, F. Herzog, J. M. Peters, D. Poerschke, R. Lührmann, H. Stark, GraFix: sample preparation for single-particle electron cryomicroscopy. *Nat Methods* **5**, 53–55 (2008).

16. H. Wang, Z. Zheng, L. Zheng, Z. Zhang, C. Dong, J. Zhao, Mutagenic analysis of the bundle-shaped phycobilisome from Gloeobacter violaceus. *Photosynth Res* **158**, 81–90 (2023).

17. K. Kawakami, T. Hamaguchi, Y. Hirose, D. Kosumi, M. Miyata, N. Kamiya, K. Yonekura, Core and rod structures of a thermophilic cyanobacterial light-harvesting phycobilisome. *Nat Commun* **13**, 3389 (2022).

18. C. J. Gisriel, G. Shen, G. W. Brudvig, D. A. Bryant, Structure of the antenna complex expressed during far-red light photoacclimation in *Synechococcus* sp. PCC 7335. *Journal of Biological Chemistry* **300**, 105590 (2024).

19. E. J. Dodson, J. Ma, M. Suissa Szlejf, N. Maroudas-Sklare, Y. Paltiel, N. Adir, S. Sun, S.-F. Sui, N. Keren, The structural basis for light acclimation in phycobilisome light harvesting systems systems in Porphyridium purpureum. *Commun Biol* **6**, 1210 (2023).

20. D. Jallet, M. Gwizdala, D. Kirilovsky, ApcD, ApcF and ApcE are not required for the Orange Carotenoid Protein related phycobilisome fluorescence quenching in the cyanobacterium Synechocystis PCC 6803. *Biochimica et biophysica acta* **1817**, 1418–27 (2012).

21. D. W. Krogmann, B. Pérez-Gómez, E. B. Gutiérrez-Cirlos, A. Chagolla-López, L. González de la Vara, C. Gómez-Lojero, The presence of multidomain linkers determines the bundle-shape structure of the phycobilisome of the cyanobacterium Gloeobacter violaceus PCC 7421. *Photosynth Res* **93**, 27–43 (2007).

22. E. Berta Gutiérrez-Cirlos, B. Pérez-Gómez, D. W. Krogmann, C. Gómez-Lojero, The phycocyanin-associated rod linker proteins of the phycobilisome of *Gloeobacter violaceus* PCC 7421 contain unusually located rod-capping domains. *Biochimica et Biophysica Acta (BBA) - Bioenergetics* **1757**, 130–134 (2006).

23. K. Tang, W.-L. Ding, A. Höppner, C. Zhao, L. Zhang, Y. Hontani, J. T. M. Kennis, W. Gärtner, H. Scheer, M. Zhou, K.-H. Zhao, The terminal phycobilisome emitter, LCM: A light-harvesting pigment with a phytochrome chromophore. *Proceedings of the National Academy of Sciences* **112**, 15880–15885 (2015).

24. G. Bernát, U. Schreiber, E. Sendtko, I. N. Stadnichuk, S. Rexroth, M. Rögner, F. Koenig, Unique Properties vs. Common Themes: The Atypical Cyanobacterium Gloeobacter violaceus PCC 7421 is Capable of State Transitions and Blue-Light-Induced Fluorescence Quenching. *Plant and Cell Physiology* **53**, 528–542 (2012).

25. A. Wilson, G. Ajlani, J. M. Verbavatz, I. Vass, C. A. Kerfeld, D. Kirilovsky, A soluble carotenoid protein involved in phycobilisome-related energy dissipation in cyanobacteria. *The Plant cell* **18**, 992–1007 (2006).

26. D. Kirilovsky, C. A. Kerfeld, Cyanobacterial photoprotection by the orange carotenoid protein. *Nature plants* **2**, 16180 (2016).

27. N. N. Sluchanko, Y. B. Slonimskiy, E. G. Maksimov, Features of Protein-Protein Interactions in the Cyanobacterial Photoprotection Mechanism. *Biochemistry. Biokhimiia* **82**, 1592–1614 (2017).

28. H. Bao, M. R. Melnicki, E. G. Pawlowski, M. Sutter, M. Agostoni, S. Lechno-Yossef, F. Cai, B. L. Montgomery, C. A. Kerfeld, Additional families of orange carotenoid proteins in the photoprotective system of cyanobacteria. *Nature plants* **3**, 17089 (2017).

29. M. R. Melnicki, R. L. Leverenz, M. Sutter, R. Lopez-Igual, A. Wilson, E. G. Pawlowski, F. Perreau, D. Kirilovsky, C. A. Kerfeld, Structure, Diversity, and Evolution of a New Family of Soluble Carotenoid-Binding Proteins in Cyanobacteria. *Molecular plant* **9**, 1379–1394 (2016).

30. F. Muzzopappa, A. Wilson, D. Kirilovsky, Interdomain interactions reveal the molecular evolution of the orange carotenoid protein. *Nature plants* **5**, 1076–1086 (2019).

31. A. Wilson, C. Punginelli, A. Gall, C. Bonetti, M. Alexandre, J. M. Routaboul, C. A. Kerfeld, R. van Grondelle, B. Robert, J. T. Kennis, D. Kirilovsky, A photoactive carotenoid protein acting as light intensity sensor. *Proceedings of the National Academy of Sciences of the United States of America* **105**, 12075–80 (2008).

32. M. G. Rakhimberdieva, I. N. Stadnichuk, I. V. Elanskaya, N. V. Karapetyan, Carotenoid-induced quenching of the phycobilisome fluorescence in photosystem II-deficient mutant of Synechocystis sp. *FEBS letters* **574**, 85–8 (2004).

33. M. Gwizdala, A. Wilson, D. Kirilovsky, In vitro reconstitution of the cyanobacterial photoprotective mechanism mediated by the Orange Carotenoid Protein in Synechocystis PCC 6803. *The Plant cell* **23**, 2631–43 (2011).

34. N. N. Sluchanko, Y. B. Slonimskiy, E. A. Shirshin, M. Moldenhauer, T. Friedrich, E. G. Maksimov, OCP-FRP protein complex topologies suggest a mechanism for controlling high light tolerance in cyanobacteria. *Nature communications* **9**, 3869 (2018).

35. Y. B. Slonimskiy, A. O. Zupnik, L. A. Varfolomeeva, K. M. Boyko, E. G. Maksimov, N. N. Sluchanko, A primordial Orange Carotenoid Protein: Structure, photoswitching activity and evolutionary aspects. *International Journal of Biological Macromolecules* **222**, 167–180 (2022).

36. N. Steube, M. Moldenhauer, P. Weiland, D. Saman, A. Kilb, A. A. Ramírez Rojas, S. G. Garg, D. Schindler, P. L. Graumann, J. L. P. Benesch, G. Bange, T. Friedrich, G. K. A. Hochberg, Fortuitously compatible protein surfaces primed allosteric control in cyanobacterial photoprotection. *Nat Ecol Evol* **7**, 756–767 (2023).

37. N. N. Sluchanko, E. G. Maksimov, Y. B. Slonimskiy, L. A. Varfolomeeva, A. Y. Bukhanko, N. A. Egorkin, G. V. Tsoraev, M. G. Khrenova, B. Ge, S. Qin, K. M. Boyko, V. O. Popov, Structural framework for the understanding spectroscopic and functional signatures of the cyanobacterial Orange Carotenoid Protein families. *International Journal of Biological Macromolecules* **254**, 127874 (2024).

38. Y. B. Slonimskiy, F. Muzzopappa, E. G. Maksimov, A. Wilson, T. Friedrich, D. Kirilovsky, N. N. Sluchanko, Light-controlled carotenoid transfer between water-soluble proteins related to cyanobacterial photoprotection. *The FEBS journal* **286**, 1908–1924 (2019).

39. Y. B. Slonimskiy, E. G. Maksimov, E. P. Lukashev, M. Moldenhauer, T. Friedrich, N. N.

Sluchanko, Engineering the photoactive orange carotenoid protein with redox-controllable structural dynamics and photoprotective function. *Biochimica et biophysica acta. Bioenergetics* **1861**, 148174 (2020).

40. R. Rippka, J. Deruelles, J. B. Waterbury, M. Herdman, R. Y. Stanier, Generic Assignments, Strain Histories and Properties of Pure Cultures of Cyanobacteria. *Microbiology* **111**, 1–61 (1979).

41. D. Tegunov, P. Cramer, Real-time cryo-electron microscopy data preprocessing with Warp. *Nat Methods* **16**, 1146–1152 (2019).

42. A. Punjani, J. L. Rubinstein, D. J. Fleet, M. A. Brubaker, cryoSPARC: algorithms for rapid unsupervised cryo-EM structure determination. *Nat Methods* **14**, 290–296 (2017).

43. E. C. Meng, T. D. Goddard, E. F. Pettersen, G. S. Couch, Z. J. Pearson, J. H. Morris, T. E. Ferrin, UCSF ChimeraX: Tools for structure building and analysis. *Protein Sci* **32**, e4792 (2023).

44. P. Emsley, B. Lohkamp, W. G. Scott, K. Cowtan, Features and development of Coot. *Acta Cryst D* **66**, 486–501 (2010).

45. K. Yamashita, C. M. Palmer, T. Burnley, G. N. Murshudov, Cryo-EM single-particle structure refinement and map calculation using Servalcat. *Acta Cryst D* **77**, 1282–1291 (2021).

46. E. G. Maksimov, M. Moldenhauer, E. A. Shirshin, E. A. Parshina, N. N. Sluchanko, K. E. Klementiev, G. V. Tsoraev, N. N. Tavraz, M. Willoweit, F. J. Schmitt, J. Breitenbach, G. Sandmann, V. Z. Paschenko, T. Friedrich, A. B. Rubin, A comparative study of three signaling forms of the orange carotenoid protein. *Photosynthesis research* **130**, 389–401 (2016).

47. D. V. Zlenko, E. A. Protasova, G. V. Tsoraev, N. N. Sluchanko, D. A. Cherepanov, T. Friedrich, B. Ge, S. Qin, E. G. Maksimov, A. B. Rubin, Anti-stokes fluorescence of phycobilisome and its complex with the orange carotenoid protein. *Biochimica et Biophysica Acta (BBA) - Bioenergetics* **1865**, 149014 (2024).

48. Z. J. Jin, [Addition in drug combination (author's transl)]. *Zhongguo Yao Li Xue Bao* **1**, 70–76 (1980).

49. F. Madeira, N. Madhusoodanan, J. Lee, A. Eusebi, A. Niewielska, A. R. N. Tivey, R. Lopez, S. Butcher, The EMBL-EBI Job Dispatcher sequence analysis tools framework in 2024. *Nucleic Acids Research* **52**, W521–W525 (2024).

50. K. Tamura, G. Stecher, S. Kumar, MEGA11: Molecular Evolutionary Genetics Analysis Version 11. *Molecular Biology and Evolution* **38**, 3022–3027 (2021).

51. D. T. Jones, W. R. Taylor, J. M. Thornton, The rapid generation of mutation data matrices from protein sequences. *Comput Appl Biosci* **8**, 275–282 (1992).

52. N. Saitou, M. Nei, The neighbor-joining method: a new method for reconstructing phylogenetic trees. *Mol Biol Evol* **4**, 406–425 (1987).

53. J. Abramson, J. Adler, J. Dunger, R. Evans, T. Green, A. Pritzel, O. Ronneberger, L. Willmore, A. J. Ballard, J. Bambrick, S. W. Bodenstein, D. A. Evans, C.-C. Hung, M. O'Neill, D. Reiman, K. Tunyasuvunakool, Z. Wu, A. Žemgulytė, E. Arvaniti, C. Beattie,

O. Bertolli, A. Bridgland, A. Cherepanov, M. Congreve, A. I. Cowen-Rivers, A. Cowie, M. Figurnov, F. B. Fuchs, H. Gladman, R. Jain, Y. A. Khan, C. M. R. Low, K. Perlin, A. Potapenko, P. Savy, S. Singh, A. Stecula, A. Thillaisundaram, C. Tong, S. Yakneen, E. D. Zhong, M. Zielinski, A. Žídek, V. Bapst, P. Kohli, M. Jaderberg, D. Hassabis, J. M. Jumper, Accurate structure prediction of biomolecular interactions with AlphaFold 3. *Nature* **630**, 493–500 (2024).

**Acknowledgements**
The authors are thankful to Prof. Alexey Amunts for help with preliminary screening of GviPBS samples on grids, to Dr. Rustam H. Ziganshin for help with running LC-MS for identification of GviPBS proteins and to Daniil M. Panin for help with OCP data analysis.
We thank Resource Center of Probe and Electron Microscopy of National Research Center ‘‘Kurchatov Institute’’ (http://rc.nrcki.ru/pages/main/nanozond/facilities/12604/index.shtml). This work has been carried out using computing resources of the federal collective usage center Complex for Simulation and Data Processing for Mega-science Facilities at National Research Center ‘‘Kurchatov Institute’’ (http://ckp.nrcki.ru).

**Funding**
This work was supported by the Ministry of Science and Higher Education of the Russian Federation (Y.B.S., K.M.B., V.O.P. and N.N.S.), Ministry of Science and Higher Education of the Russian Federation theme no.122042700045-3 (M.A.S.) and the Russian Science Foundation grant 23-74-00062 (A.D.B.).

**Author contributions**
Conceptualization: NNS
Methodology: ADB, YBS, TNB, EGM, VOP, NNS
Investigation: ADB, YBS, TNB, MAS, DAG, GVT, DAC, EGM, KMB, NNS
Visualization: ADB, YBS, EGM, NNS
Funding acquisition: MAS, VOP, KMB, NNS
Project administration: NNS
Supervision: KMB, NNS
Writing – original draft: NNS
Writing – review & editing: NNS, with input from all authors

**Declaration of competing interests**
The authors declare no conflicts of interest.

**Data availability**
The atomic coordinates have been deposited in the Protein Data Bank with the accession codes 9V7J (PBS core), 9V7K (PBS C), 9V7G (PBS Rx), 9V7L (PBS R1), 9V7H (PBS R2) and 9V7I (PBS R3). The cryo-EM maps have been deposited in the Electron Microscopy Data Bank with accession codes EMD-64815 (PBS core), EMD-64816 (PBS C), EMD-64812 (PBS Rx), EMD-64817 (PBS R1), EMD-64813 (PBS R2), EMD-64814 (PBS R3), EMD-64828 (consensus), EMD-64868 (composite), EMD-64851 (diverging rods) and EMD-64852 (parallel rods). Raw time-resolved emission spectra for GviPBS in the absence or in the presence of GviOCP3a_α, GviOCP3a_β, or their combination have been uploaded to Zenodo (https://doi.org/10.5281/zenodo.15575709). Other data are available in the paper or in Supplementary information.

**Supplementary information**

Materials and Methods

Tables S1-S2

Figures S1-S19

Movie S1

## Figures and legends

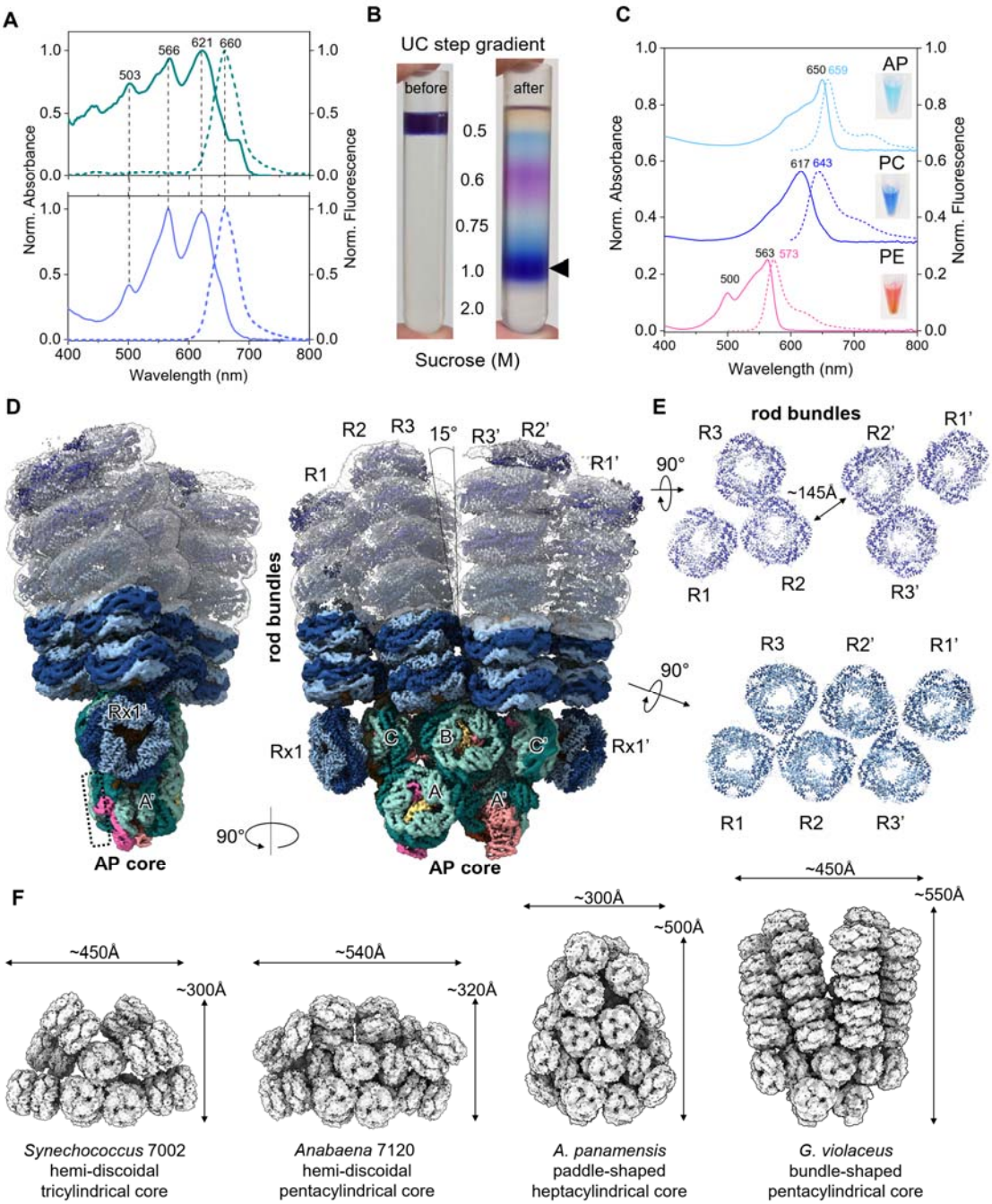


**Fig. 1. The bundle-shaped phycobilisome from *G. violaceus*. A**. Absorption (solid line) and fluorescence (dashed line) spectra of *Gloeobacter* cells (top) and isolated PBS (bottom). An integrating sphere was used to measure the absorption spectrum of the cells. In both cases, fluorescence was excited at 630 nm. **B**. PBS isolation by ultracentrifugation in sucrose gradient as shown. Arrow indicates the PBS zone. **C**. Absorption (solid line) and fluorescence (dashed line) spectra of the individual allophycocyanin (AP), phycocyanin (PC) and phycoerythrin (PE). Excitation was at 475 (PE) or 575 nm (PC, AP). The samples are shown in insert. **D**. Composite cryo-EM map of the bundle-shaped PBS showing the location

of the AP core (A/A', B and C/C' cylinders) and rod bundles. **E**. Sections across the rods on the two levels indicated by arrows, showing diverging three-rod bundles R1-R2-R3 and R1'-R2'-R3'. **F**. Cryo-EM structures representing the relative sizes of different cyanobacterial PBS – hemi-discoidal PBS from *Synechococcus* and *Anabaena* (*8*), paddle-shaped PBS from *A. panamensis* (*5*) and bundle-shaped PBS from *G. violaceus* PBS (this work).

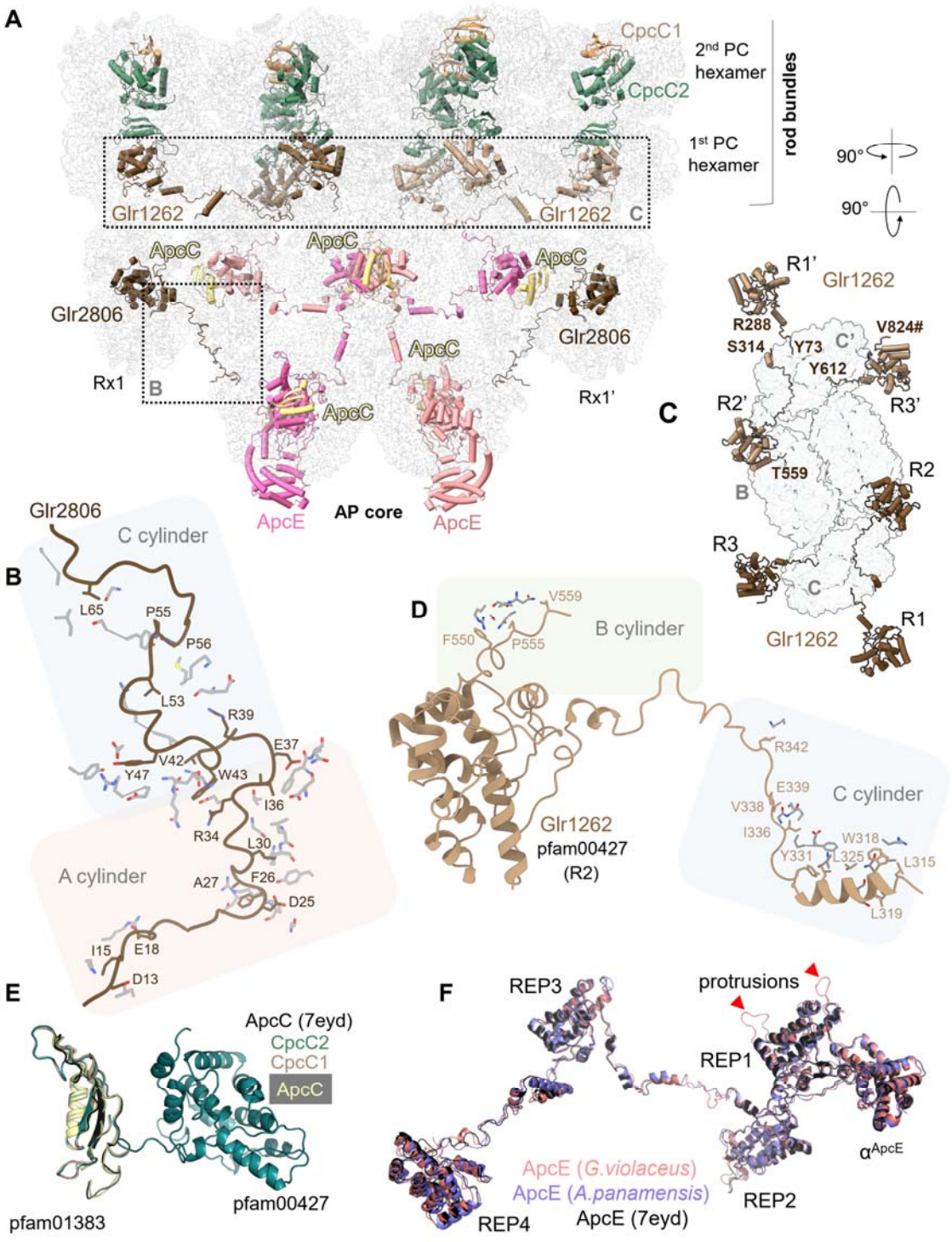


**Fig. 2. Linker proteins of GviPBS. A**. Front view of the AP core and two PC levels in the rods. PBP hexamers are shown as semitransparent ribbons, linker proteins are in cartoon representation. All linkers are labeled except for CpcC1/CpcC2 for which only one copy is labeled. Parts of the model for focused analysis in separate panels are framed. **B**. Contacts formed by the N-terminal arm of Glr2806 with the core cylinders A/A' and C/C'. **C**. Topology of the two copies of Glr1262 on top of the core showing relative positions of the repeat

domains REP1, REP2, REP3 that attach bases of the rods R1/R1', R2/R2', R3/R3', respectively, by clustering them as two rod bundles. # indicates the C terminal of the Glr1262 chain. **D**. Contacts made by the arms of Glr1262 with the core cylinders B and C/C'. **E**. Superposition of ApcC capping linker of *G. violaceus* with ApcC from Anabaena PBS (PDB 7eyd) and with the equivalent pfam001383 domains of CpcC1 and CpcC2 rod linkers. **F**. Superposition of ApcE from *G. violaceus*, *A. panamensis* and *Anabaena* 7120 showing the location of the REP1-4 domains and the bilin-binding $\alpha^{ApcE}$ domain. The profound difference is the presence of large unstructured protrusions exclusively in REP1 of *G. violaceus* ApcE (indicated by red arrows).

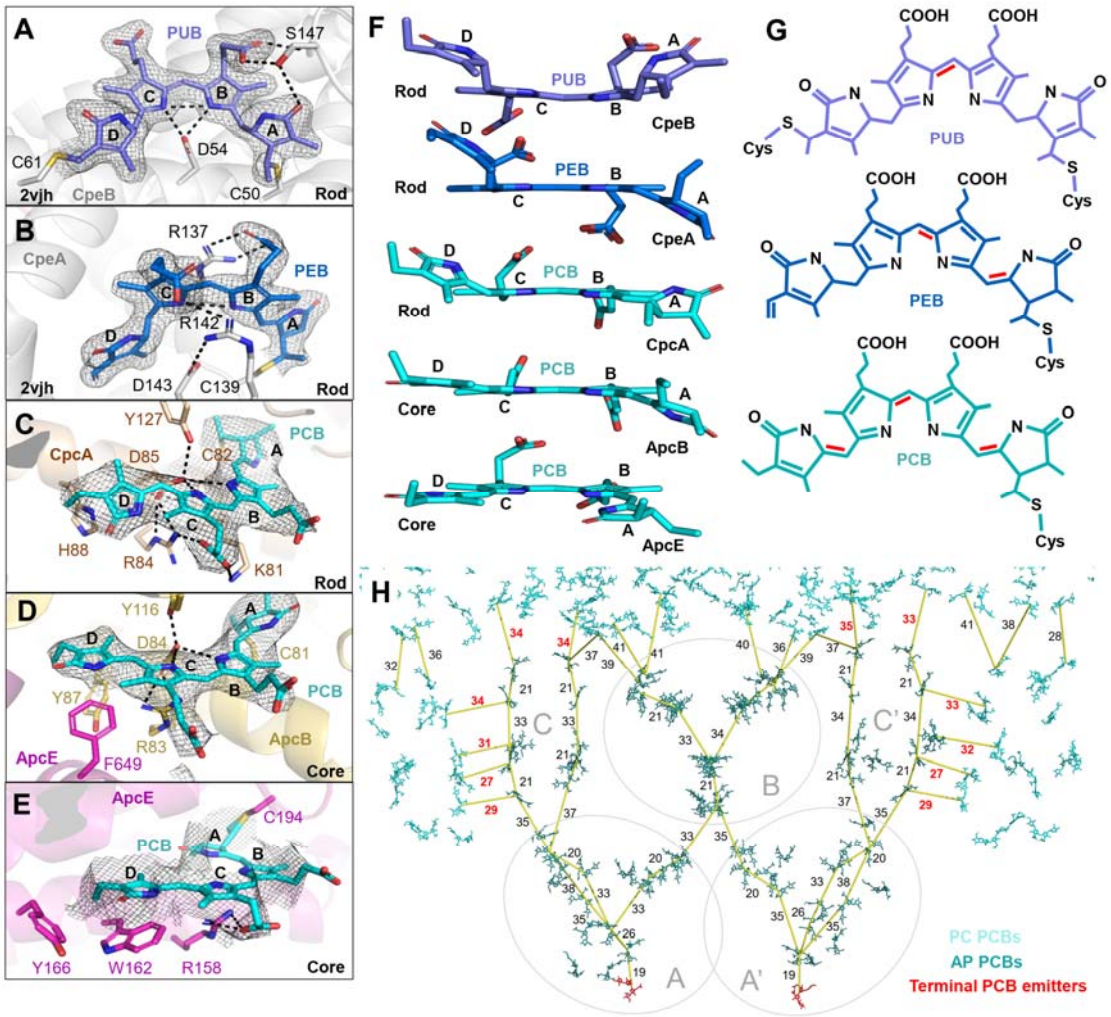


**Fig. 3. Bilins of GviPBS. A-E.** Representative PUB, PEB and PCB bilin conformations, shown with the polar contacts to the surrounding protein residues and the respective electron density (1σ contour). PUB and PEB binding sites are imaged using the crystal structure of PE (PDB 2vjh), PCB sites are from cryo-EM data obtained in this work. **F**. Coplanarity of the bilins shown in panels **A-E**. Pyrrole rings A-B-C-D are labeled. **G**. Structures of the three bilin types found in GviPBS. Red lines mark the distinctive double bonds connecting the pyrroles. **H**. Estimation of the EET pathways from PC to AP and within AP in GviPBS. Distances connecting mass centers of the selected PCBs are indicated in Å by yellow lines. Remarkable shortest distances (≤35 Å) between PC and AP bilins are indicated by red font. Terminal emitting bilins of ApcE are shown by red sticks.

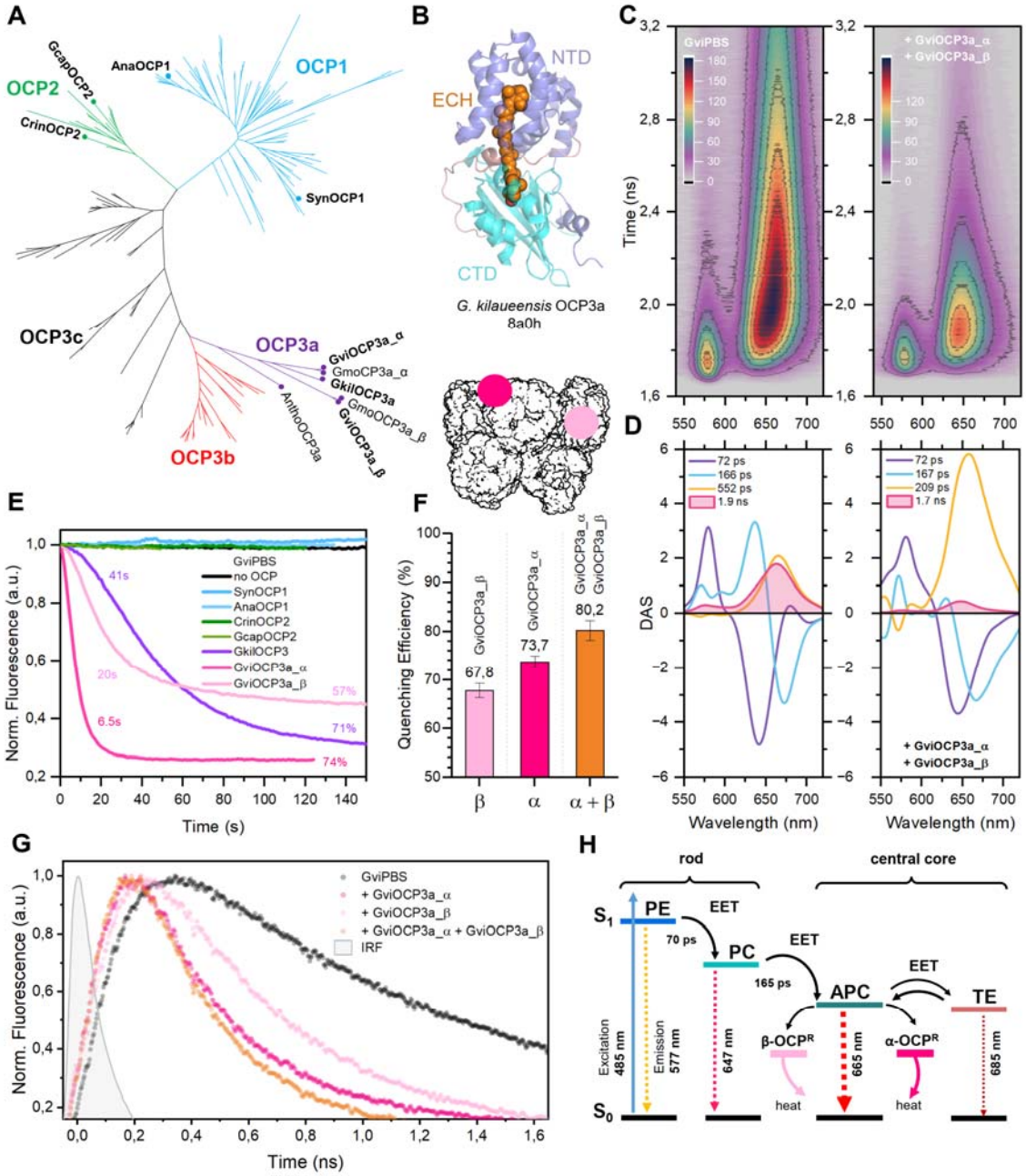


**Fig. 4. Quenching of GviPBS by orange carotenoid proteins. A**. Phylogenetic tree showing the relationships between OCP1, OCP2, OCP3a, OCP3b and OCP3c clades. OCP homologs considered in this work are labeled. Construction of the tree is described in detail in Methods. **B**. Crystal structure of OCP3a from *G. kilaueensis* (*35*) showing the location of its NTD and CTD domains and the embedded echinenone (ECH) chromophore required for photoactivity. **C**. Time-resolved emission spectra (TRES) of GviPBS fluorescence in the absence and presence of the combination of GviOCP3a_α and GviOCP3a_β. **D**. Decay associated spectra (DAS) of GviPBS fluorescence data presented in **C**. The numbers indicate characteristic kinetic components derived from the global analysis of time-resolved fluorescence spectra (**C**) showing the response to photoactivation of GviOCP3a_α and GviOCP3a_β in combination. **E**. Time-courses of GviPBS quenching by OCP variants,

showing characteristic time constant of 2-fold reduction of fluorescence and overall quenching efficiency. **F**. Quenching efficiency estimated as a relative reduction of yield of c.a. 1.8 ns components upon the photoactivation of GviOCP3a_α and GviOCP3a_β and their combination based on global analysis of TRES (C). **G**. Normalized fluorescence decay kinetics of GviPBS at 680 nm excited by 150 fs laser pulses at 485 nm. The temperature of the samples was stabilized at 10 °C during all experiments to prevent fluorescence recovery. **H**. Schematic description of the excitation energy transfer (EET) processes within GviPBS and the effect of GviOCP3a_α and GviOCP3a_β on dissipation of the absorbed energy.